Engineering Journal issn: 0125-8281

Article

Study of Microstructure and Mechanical Properties of Commercially Pure Sn and Sn-4%Bi Alloys Fabricated by Permanent Mold Gravity Casting and Forging

Chonnakan Thongchai[1,a], Boonrat Lohwongwatana[1,b,*], Chedtha Puncreobutr[1], Atchara Khamkongkaeo[1], Thanawat Phetrattanarangsi[1], Burimpak Sakkomolsri[2], Pinit Kidkhunthod[3], and Narong Chanlek[3]

1 Innovative Metals Research Unit, Department of Metallurgical Engineering, Faculty of Engineering, Chulalongkorn University, Bangkok 10330, Thailand
2 Department of Physics, Khon Kaen University, Khon Kaen 40002, Thailand
3 Synchrotron Light Research Institute, Nakhon Ratchasima 30000, Thailand
E-mail: [a]chonnakan.thongchai@gmail.com, [b]boonrat@gmail.com (Corresponding author)

Abstract. The influences of 4 wt% bismuth addition and room temperature strain on microstructure and mechanical properties in tin alloys were investigated in this study. Commercially pure tin and Sn-4%Bi alloys were fabricated by permanent mold gravity casting. The samples were then subjected to forging process at room temperature. As-cast microstructures were compared with 0.25 and 0.5 strained samples. Differential Scanning Calorimetry (DSC) was used to confirm the effect of bismuth on undercooling. The recrystallization and grain growth processes were confirmed by grain size distribution and misorientation study using Electron Backscattered Diffraction (EBSD). Furthermore, position and morphology of the bismuth precipitates were investigated by using Field Emission Scanning Electron Microscope (FESEM). X-ray Photoelectron Spectroscopy (XPS) revealed that tin oxide was the main species found on the surface of these alloys. There was no evidence of bismuth oxide on the surface. Furthermore, the Hall-Petch hardness approximation analysis revealed that there were other influences, which increased the hardness beyond the grain refinement effect.

Keywords: Tin, bismuth, forging, recrystallization, permanent mold casting, lapping plate.

ENGINEERING JOURNAL Volume 22 Issue 5
Received 30 July 2017
Accepted 23 July 2018
Published 30 September 2018
Online at http://www.engj.org/
DOI:10.4186/ej.2018.22.5.171

DOI:10.4186/ej.2018.22.5.171

1. Introduction

Sn-Bi alloys are widely used in many applications in electronics industry owing to their mechanical properties that match well with the needs in the areas such as lapidary, soldering, coating, etc. Along with Sn-Ag-Cu alloy systems for soldering applications, Sn-Bi alloys have also been considered as low-cost and environmentally friendly lead-free solders [1]. In one specific application in an electronic industry, Sn-Bi alloys are currently used as lapping plate material in hard disk drive manufacturing process. Such process subjects the read-write heads of hard disk drive to prolonged, intimate, and mechanically abrasive contacts to Sn-Bi alloys without altering the magnetism and read-write properties of the hard disk drive heads [2, 3]. Lapidary process is currently adopted throughout the electronic manufacturing industry in which smooth surface is required for aesthetic and/or engineering reasons.

With the melting point at 504.9 K, tin creeps at near-ambient temperature. It is well known that recrystallization temperature of Sn and many of its alloys are near or below room temperature. As most manufacturing processes are commonly carried out at room temperature, in which the mechanical properties of tin alloys become inevitably dynamic, detailed characterization of room-temperature effects on tin and its alloys are required.

In one particular example, Sn-Bi lapping plate is subjected to a process commonly known as diamond charging prior to mechanical lapping process. Slurry filled with micron level abrasive diamonds is poured on top of lapping plates while hard ceramic charging wheel drives the diamonds mechanically into the soft tin land-area. Microstructural evolution of lapping plate is therefore, one of the most important factor for effective diamond charging. Microstructural refinement of Sn alloys has therefore been central in Sn-alloys research during the past recent years. One of the effective ways to achieve microstructure refinement is the addition of alloying element(s). For example, the addition of Co in Sn-Ag-Cu solder results in a formation of intermetallic $CoSn_3$ particles in molten alloy, which thereby act as nucleation sites for βSn grains [4]. Addition of Mn in Mg-Zn-Ca alloy will also cause grain refinement but the controlling mechanism related to constitutional undercooling [5]. Furthermore, there are other processes that can be effectively used to refine the final microstructure including increasing the rate of cooling or rapid quenching [6], severe plastic deformation [7], hot forging [8], etc. There are also many indirect factors that improve embedding of diamond in charging process such as rotational rate of ceramic ring which is used for driving diamond abrasives into lapping plate, rotational rate of lapping plate, as well as temperature during charging, etc.

Particularly for Sn-Bi alloy system, the bismuth solid solubility in tin is approximately 1-2 wt% Bi at room temperature. Such compositional range for Bi in tin was observed in the β-Sn phase found in eutectic microstructure. Insights of such tin alloy compositions and related mechanical properties are important to both solder application for stress-relieving purpose and lapidary application for restricted work hardening of lapping plate.

2. Experimental Procedure

Commercially pure Sn (denoted as 'pure Sn') and Sn-4%wtBi alloy were prepared using induction melting. The actual chemical composition of each alloy was analyzed by X-ray fluorescence (XRF), and the results as shown in Table 1. Specimens were produced by permanent mold gravity casting in borosilicate glass crucible at 573K (300°C), following by slow cooling down in ambient atmosphere. In order to control the equivalent final dimension of forged samples which were subjected to various strains, each sample was casted to different initial dimensions: 10 mm diameter by 2 mm thickness, 8.7 mm diameter by 2.67 mm thickness, and 7 mm diameter by 4 mm thickness. The samples were prepared for both commercially pure Sn and Sn-4%wtBi alloy. After casting, 8.7 mm and 7 mm in diameter samples were forged in die as shown in Fig. 1. The final dimension of forged samples has 10 mm diameter and 2 mm in thickness as shown in Fig. 2. These two samples were labeled 0.25 and 0.5 strain samples respectively.

The samples were forged by a hydraulic machine with 200 kN load at 303 K, and were prepared for microstructure investigation by grinding with abrasive papers, with grit size of 120, 240, 360, 600, 800 and 1200 respectively. The samples were subsequently polished with aluminum oxide 1 μm and diamond powder suspension 0.1 μm respectively. Then, all samples were etched by 5%vol nitol acid (5%vol nitric acid with methanol) for 10 second. After etching with nitol acid, only Sn-4%wtBi alloy samples were etched by 3%vol hydrochloric acid with methanol for 20 second. Along the preparation and characterization processes, the samples were conserved in desiccator at 298 K.

DOI:10.4186/ej.2018.22.5.171

Table. 1. The composition of two alloys that use as raw material.

Raw material	Weight percent										
	Sn	Pb	As	Bi	Cu	Fe	Ag	Sb	Zn	Cd	Al
Commercially pure Sn	99.918	0.032	0.006	0.018	0.006	0.005	<0.001	0.008	<0.001	<0.001	<0.001
Sn4%wtBi	95.83	0.021	<0.010	4.12	0.006	0.003	<0.001	0.005	<0.001	<0.001	<0.001

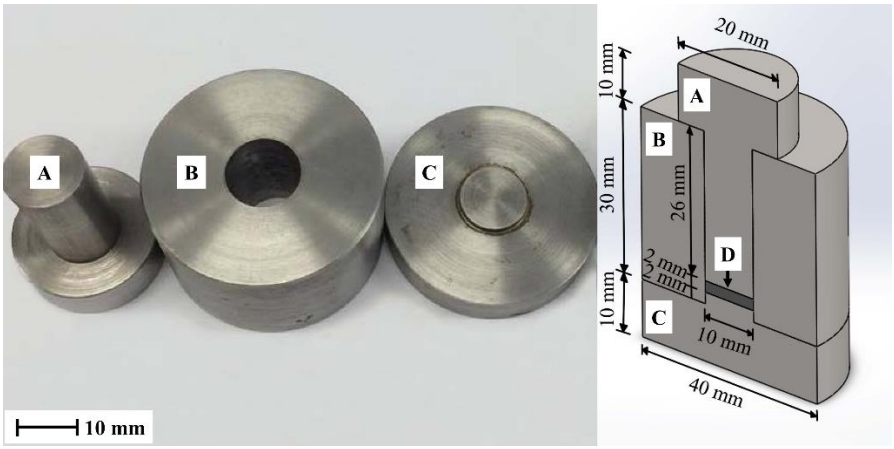

Fig. 1. Image of the actual die parts are shown on the left. Cross sectional schematic of assembled die parts is shown on the right with forged specimen (D).

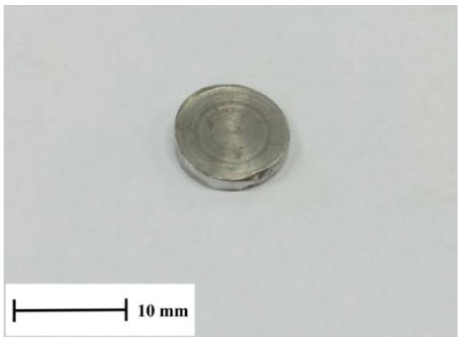

Fig. 2. Example of forged sample.

After the preparation of the samples, the microstructure was investigated by an optical microscope (OM) to quantify number of grains and average grain size. To investigate further the bismuth precipitate morphology and their localities in the microstructure of Sn-4%wtBi alloy samples, Field Emission Scanning Electron Microscope (FESEM) (JSM-7001F, JEOL) and Energy Dispersive X-Ray Spectrometer (EDS) (INCA PentaFETx3, Oxford) were used. In order to understand the effect of bismuth addition on microstructure and melting behavior, pure tin and Sn-4%wtBi alloy samples were analyzed by Differential Scanning Calorimetry (DSC) (Netzsch STA449 F3 Jupiter thermal analyzer, Germany) to observe their undercooling characteristics. Furthermore, X-Ray Diffraction (XRD) was used for preliminary investigation of crystal structure, followed by Electron Backscattering Diffraction (EBSD) investigation. For recrystallization and grain growth, EBSD was used to investigate the orientation of microstructure as well as its misorientation angle distribution. The hardness of all samples was compared by Vickers Hardness to compare the effects of microstructure and the mechanical properties of the samples. The species of oxides

on the surface that occur during casting and during storage were investigated by X-Ray Photoelectron Spectroscopy (XPS). Time spent for sample preparations was approximately 4 weeks.

3. Results and Discussion

As-cast and the as-forged or strained microstructures of all samples are shown in Fig. 3. The grain size was analyzed by using ASTM standard with planimetic method [9]. For magnification 50X OM images of pure Sn samples, Jeffries's Multiplier (f) equals 0.5. For magnification 200X OM images of Sn-4%wtBi alloy samples, Jeffries's Multiplier (f) equals 8.0.

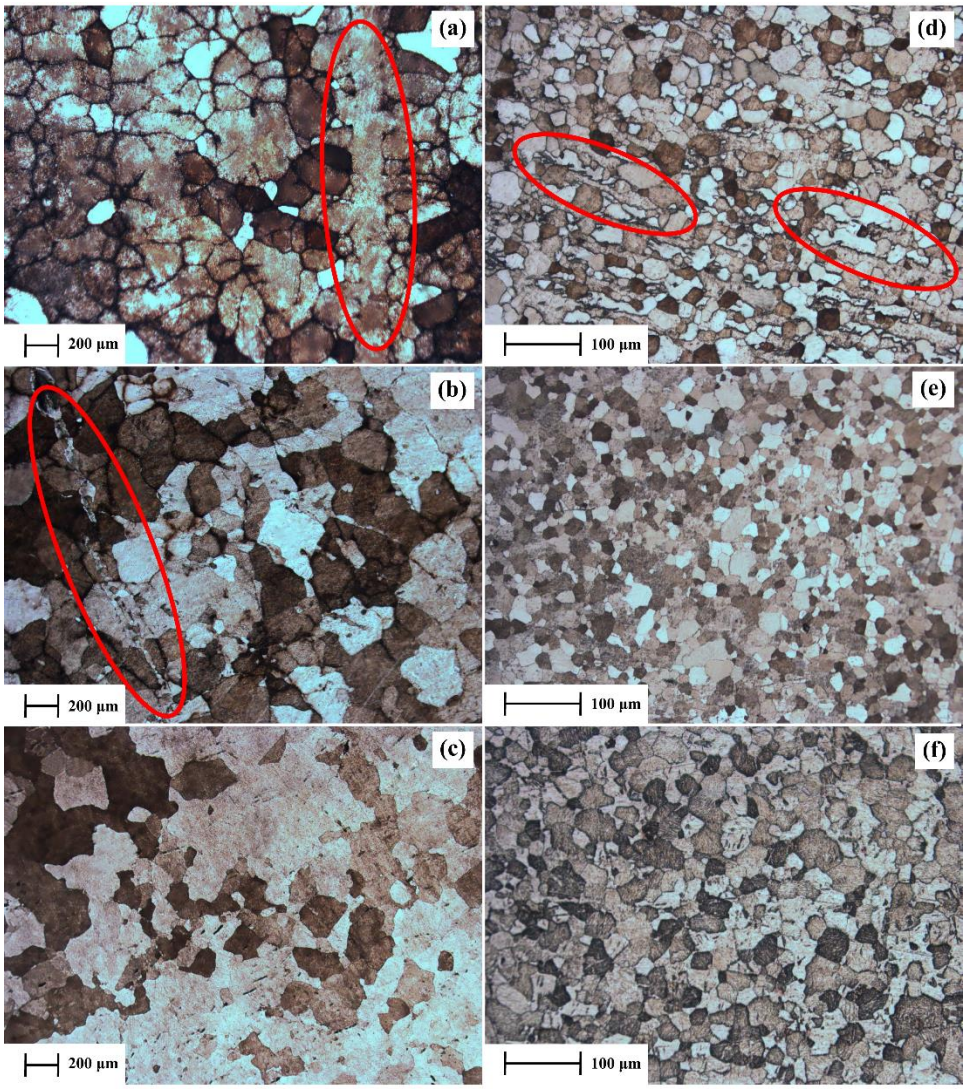

Fig. 3. Optical microstructure images of pure Sn (a, b, c) and Sn-4%wtBi alloy (d, e, f). As cast samples were indexed with (a) and (d). 0.25 strain samples were indexed with (b) and (e), finally 0.5 strain samples were indexed with (c) and (f).

Both of as-cast samples revealed a microstructure comprising mainly of tin-rich phase and almost pure bismuth precipitates were found along grain boundary in some area as confirmed by SEM-EDX qualitative analysis. The finding is in good agreement in the microstructure previously reported literatures such as R. Mahmudi *et al.* [10]. According to H.Okamoto [11], the solubility limit of Bi in Sn is approximately 1.5-2 wt% at room temperature. The solubility of Bi reaches maximum of 21 wt% at 139 C and sharply drops with temperature. It could then be expected that, under normal cooling condition, Bi atoms remain in both beta tin-rich matrix while some Bi precipitates would decorate along the grain boundary in the case of Sn-4%wtBi

alloy. The grain size of as-cast Sn-4%wtBi alloy was found to be finer than pure Sn. The average grain sizes of as-cast pure Sn and Sn-4%wtBi alloy samples were 191 μm and 22 μm respectively.

It is well established that nucleation of β-Sn from Sn-base liquid alloys is generally difficult [12] since sufficient driving force (Gibbs free energy) is required to create high energy solid/liquid interface for a stable nuclei formation. This agrees well with the DSC result in this study, shown in Table 3, that undercooling of 17.3 K is required for pure Tin. In case of Sn-4%wt.Bi alloy, as the solid β-Sn interface advances the concentration of the rejected Bi element in the liquid adjoining the interface is increased and its local freezing temperature reduced. This effect is well known as constitutional undercooling. With this solute buildup ahead of solid/liquid interface, the total undercooling is further increased. This could be confirmed by DSC result shown in Table 3 where the undercooling of 25.9 K is required for the Sn-4%wt. Bi alloy. With this increased undercooling, the liquid has to cool further before the solidification could proceed and thus allow for additional driving force for the activation of other nuclei. This results in the increased rate of nucleation and the more grains would be expected in the final solidified microstructure.

Previous work also proposed a Growth Restriction Factor (GRF) which is a measure of the extent to which the advance of the solid interface into the adjoining liquid under the influence of a temperature gradient is limited by the increase in solute concentration in the area adjacent to the interface. K. Sweatman *et al.* [13] reported that addition of Bi could increase GRF in the Sn-based alloy.

According to Table 2, the grain sizes of 0.25 strain samples for both compositions were finer than that of as-cast samples. During a straining process at room temperature, a fraction of mechanical energy was stored in the forged specimen in the combinations of vacancy defects, interstitial defects, dislocations and stacking faults. However such stored energy of deformation is mainly stored in the form of dislocations. In our case, there were three main mechanisms driven by stored deformation energy: recrystallization, grain coarsening and recovery. Recrystallization [14] refers to a process to form a new grain following the formation, and migration of high angle grain boundaries. Recovery is defined [15] as all processes involving the release of energy outside the realm of high angle grain boundary movement, except for the case of mean grain size increase driven by reduction of grain boundary area and energy associated [16]. Because of the low recrystallization temperature of these alloys, recovery and dynamic recrystallization could occur [17] in addition to microstructural homogeneity of as-forged samples.

Table. 2. The grain size numbers and average grain sizes (μm) of the alloy samples at various strain.

Samples		grain size No.	average diameter (μm)
pure Sn	as cast	1.827	191
	0.25 strain	2.999	127
	0.5 strain	1.904	186
Sn-4%wtBi	as cast	8.012	22
	0.25 strain	8.838	16
	0.5 strain	7.133	30

For the case of pure Sn, the mean grain size was 191 micrometer as-cast, then reduced to 127 micrometers at 0.25 strain, and increased to 186 micrometers following 0.5 strain. For the case of Sn-4%wtBi, the mean grain size was 22 micrometers, reduced to 16 micrometers for 0.25 strain, then increased to 30 micrometers following 0.5 strain. It is well-known that the recrystallization temperature of pure tin is relatively low, therefore the samples should be carefully kept during sample preparation process. These grain size values lie within the range of previously reported values from the literature which confirmed that the samples were not completely recrystallized along the process. In order to understand the mechanism underlying the change of mean grain size, the distribution of high and low angle grain boundaries could shed more lights on the mechanisms involved.

Broadly speaking, the system tended to reduce internal energy by reducing grain boundaries [18]. However the processes involved during the recrystallization could be separated in multiple steps. For example, following Cottrell [19], critical factor included pre-existing subgrains that were localized and highly misoriented angles. Such high angle grain boundaries had sufficient mobility to evolve into new strain-free grains. Dislocation density difference on both sides of the grain boundary could drive atoms from a more perfect grain into the less perfect grain. Such grain boundary movement could annihilate dislocations and

create also small strain-free volume. In the laboratory timescale of approximately 20 days, the microstructure of all 0.5 strain samples was already altered.

To investigate crystal structure and extent of alteration of these specimens, all samples were analyzed by using X-ray diffraction study, followed by EBSD analysis. The main crystal system was found to be tetragonal. Space group number and space group were 141 and $I4_1/amd$. Lattice parameter (a, b, c) were agreeable with 0.58332 nm, 0.58332 nm and 0.31820 nm respectively as reported in [20].

Orientation imaging microscopy (OIM) maps and misorientation angle distribution of as-cast, 0.25 strain and 0.5 strain of Sn-4%wtBi alloy samples were shown in Fig. 4. The as-cast distribution showed a degree of preferred orientation which may be contributed by the texturing effect of small-volume casting. When compared to as-cast microstructure, the reduction in size was reported in Fig. 4(c) at approximately 16-18 micrometers. Figure 4(d) indicated the broadening in misorientation angle distribution which resembled that of a random distribution such as the distribution simulations by Mason *et al.* [21] and Mishin *et al.* [22]. The reason for such random distribution remains inconclusive whether or not recrystallization was indeed taken place. Textured structure was not evident in the intermediate case of 0.25 strain. This may be because the recrystallization process does not generate preferred orientation if the pinning effect. As reported by Doherty *et al.* [15] when a primary phase represented a large volume fraction and a secondary phase particles could pin grain boundaries, recrystallization process does not always end in a preferred orientation.

As for the case of 0.5 strain samples, the mean grain size was increased while grain boundary misorientation distribution decreased significantly towards lower angles. Clusters of grains of similar shades are shown in Fig. 4(e) which suggest that new grains grow from many smaller regions already present in deformed microstructure. The result agrees with reported findings such as [23] and [24].

From the metallographic perspective, electron backscattered imaging in SEM/EDS was used to investigate the morphology and position of bismuth precipitates. The SEM/EDS images of Sn-4%wtBi alloy samples in Fig. 5 revealed the morphology of bismuth precipitates. The bright areas in SEM backscattering images were identified as bismuth precipitates. The gray area in SEM backscattering image was identified as β-Sn matrix. Bismuth precipitates of as cast and 0.25 strain samples were found along the grain boundaries (GBs). In the majority of as-cast samples, it was confirmed that Bi precipitated along the GBs after the solidification of β-Sn matrix. On the other hand, many Bi precipitates of 0.5 strain samples were found in the middle of grains, which can be linked to the grain growth following the recrystallization process as discussed earlier.

In order to investigate the effect of bismuth on undercooling, it is necessary that the two compositions of the Sn alloys be analyzed by using Differential Scanning Calorimetry (DSC). The DSC curves of heating and cooling processes were shown in Fig. 6. The increase in undercooling is usually indicated by the difference between the onset temperatures of heating process $T_{onset}(heating)$ and the onset temperatures of cooling process $T_{onset}(cooling)$, as shown in Eq. (1). At any given temperature below melting point, nucleation is initiated by the driving force for solidification (ΔG_V), which would increase if undercooling increased. However, there is an interfacial energy (γ^{SL}) which is a kinetic barrier for nucleation. Thus, Gibbs free energy of homogeneous nucleation is equal to negative term of driving force for solidification and positive term of kinetic barrier. Critical radius of nuclei which is large enough to be nucleation sites that could be estimated by the differential of Gibbs free energy. Equqation (2) represents the critical nuclei size (r*) which is a relative function of the latent heat of fusion (ΔH_s), the undercooling (ΔT), and the melting point (T_m). Also, nucleation barrier energy (ΔG^*) equation could be obtained by substituting critical nuclei in Gibbs free energy equation. However, the nucleation, which usually occur in nature, is a heterogeneous nucleation. It always has other surface that can be a nucleation side such as container walls, impurity particles, grain boundary etc. As heterogeneous nucleation is also related to homogeneous nucleation, Gibb free energy of heterogeneous nucleation was estimated, as shown in Eq. (3). According to Eq. (2) and Eq. (3), the critical nuclei size and nucleation barrier would be decreased when (ΔT) is increased.

The values from thermal analysis are shown in Table 3 along with latent heat of fusion for solidification (ΔH_s) which was derived from integration of area under a DSC curve during cooling process. The result confirmed that the undercooling was increased from 17.3 K in pure Sn to 25.9 K in Bi-contained Sn alloy. Thus, the addition of Bi potentially increased driving force for nucleation and thus promoted grain refinement.

DOI:10.4186/ej.2018.22.5.171

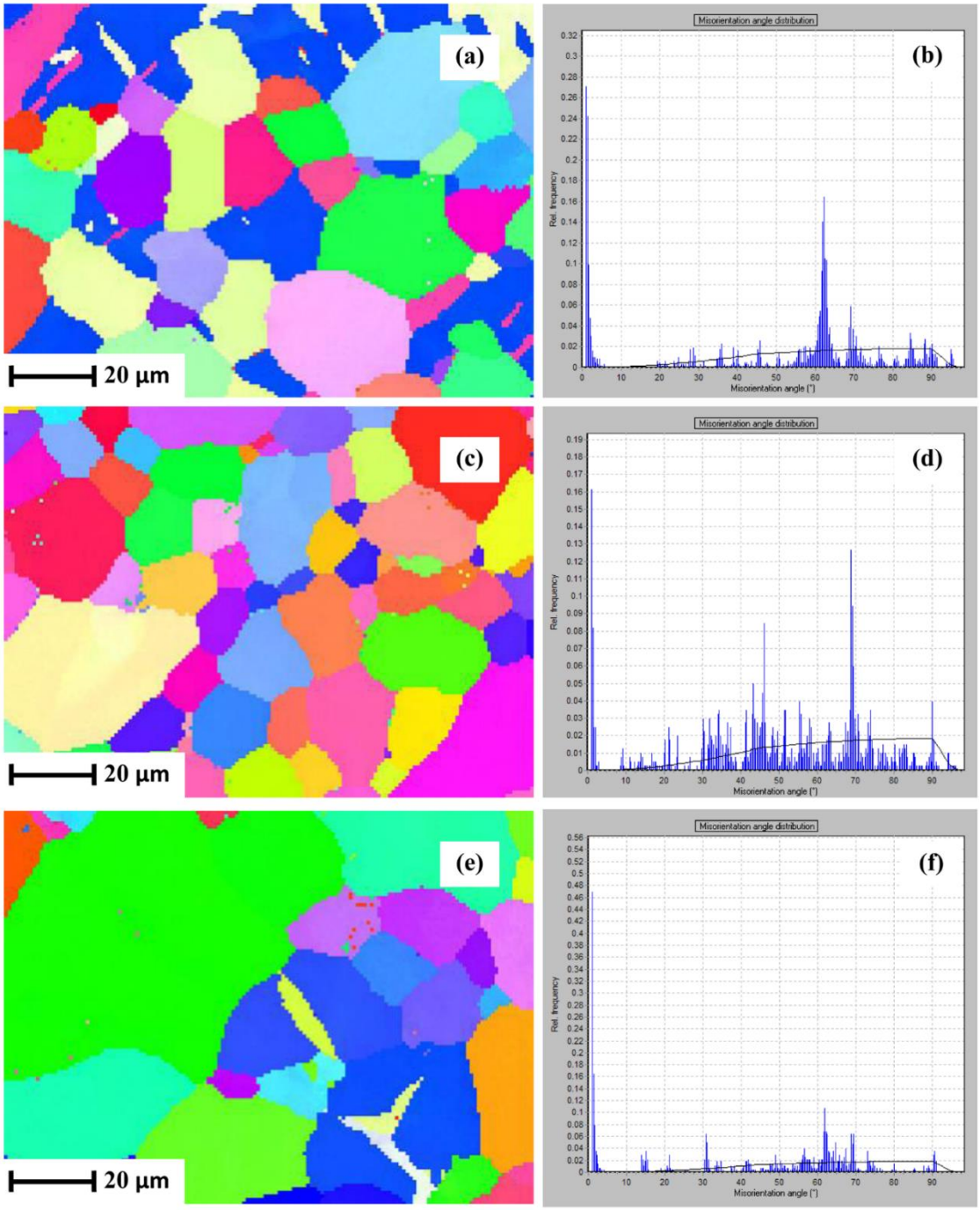

Fig. 4. The orientation imaging microscopy (OIM) maps from EBSD analysis maps and misorientation angle distribution of as-cast (a, b), 0.25 strain (c, d) and 0.5 strain (e, f) Sn-4%wtBi alloy samples.

DOI:10.4186/ej.2018.22.5.171

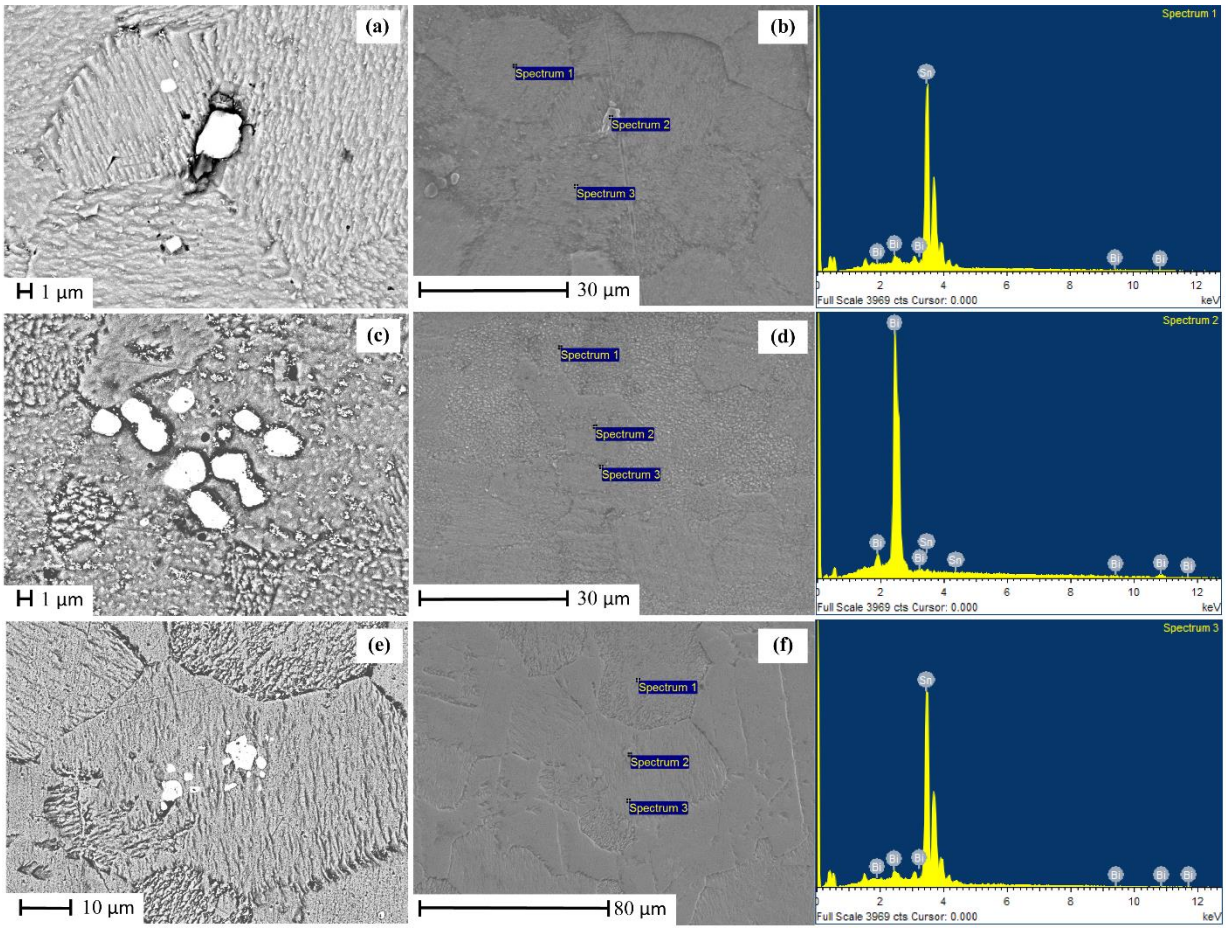

Fig. 5. SEM images and EDS points analyzed images of as cast (a, b), 0.25 strain (c, d) and 0.5 strain (e, f) Sn-4%wt.Bi alloy samples.

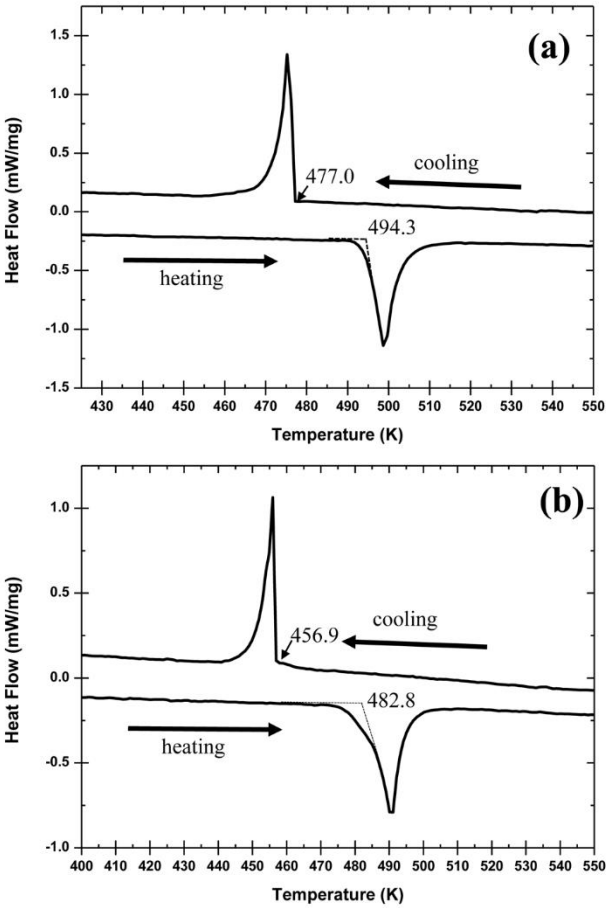

Fig. 6. The DSC curves show onset temperature during heating and cooling of (a) pure Sn and (b) Sn-4%wtBi alloy samples.

Table. 3. The result of DSC analyzation.

Alloys	$T_{onset}(heating)$ (K)	$T_{onset}(cooling)$ (K)	undercooling (K)	ΔH_s (j/g)
pure Sn	494.3	477.0	17.3	65.23
Sn-4%wtBi	482.8	456.9	25.9	64.77

$$\Delta T = T_{onset}(heating) - T_{onset}(cooling) \quad (1)$$

$$r^* = \left(\frac{2\gamma^{SL}T_m}{\Delta H_s}\right)\frac{1}{\Delta T} \quad (2)$$

$$\Delta G^*_{het} = \left(\frac{16\pi(\gamma^{SL})T_m^2}{3(\Delta H_s)^2}\right)\frac{1}{(\Delta T)^2}\, s(\theta) \quad (3)$$

Furthermore, the hardness of all samples was compared using Vickers hardness tester in order to understand the relationship between the effects of microstructure and the mechanical properties. The Vickers hardness result of all samples were showed in Fig. 7. According to Hall-Petch relations as shown in Eq. (4) [25, 26], the hardness of both compositions of as-cast alloys was improved after forging at 0.25 strain. After forging at 0.5 strain, as the microstructure of the alloys became coarser as earlier reported by EBSD and SEM analysis, the hardness values decreased as expected. Such range of hardness values confirmed that the specimens were in recovered state with similar amount of stored deformation energy. Figure 8 shows

hardness values that were plotted from Hall-Petch relation, comparing to experimental hardness. It was shown that hardness of pure Sn samples followed the hardness projection using Hall-Petch relation. On the other hand, measured hardness of Sn-4%wt.Bi alloy samples was 45-50% higher than the hardness trend as suggested by Hall-Petch relationship. This suggests that grain boundary strengthening is not the only mechanism. In addition to the aforementioned mechanism, there are also the effects of solid solution strengthening and precipitation strengthening.

$$H_v = H_0 + \frac{k}{\sqrt{d}} \tag{4}$$

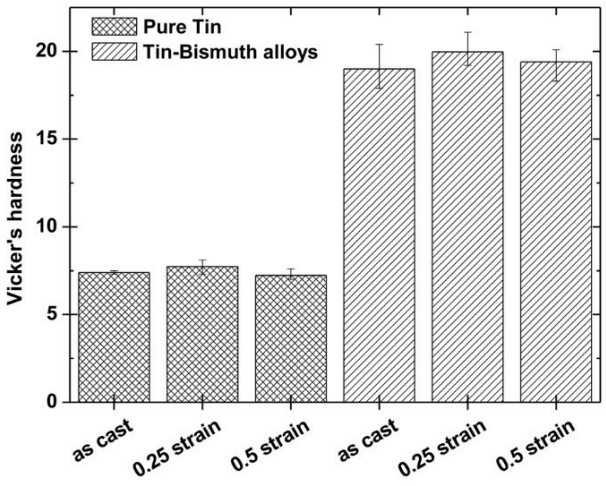

Fig. 7. Diagram shows Vicker's hardness of pure Sn and Sn-4%wtBi alloy samples at different strain.

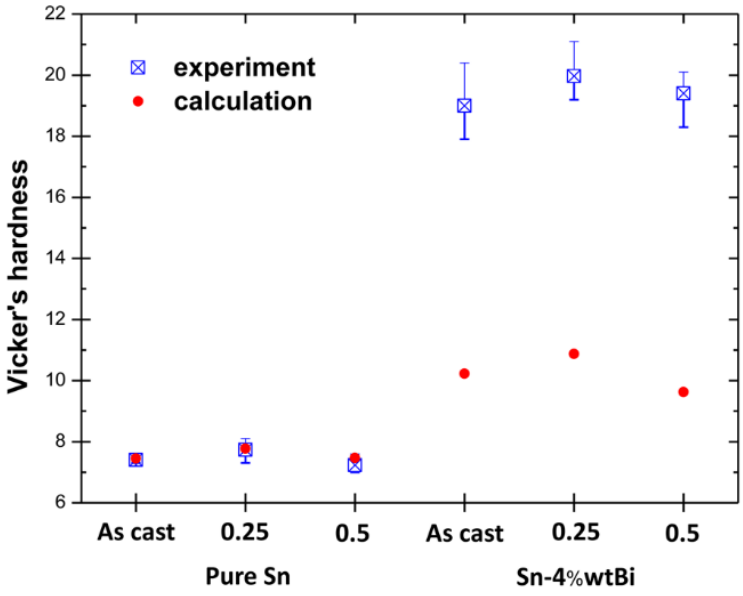

Fig. 8. Diagram shows comparison between experimental hardness and calculating hardness.

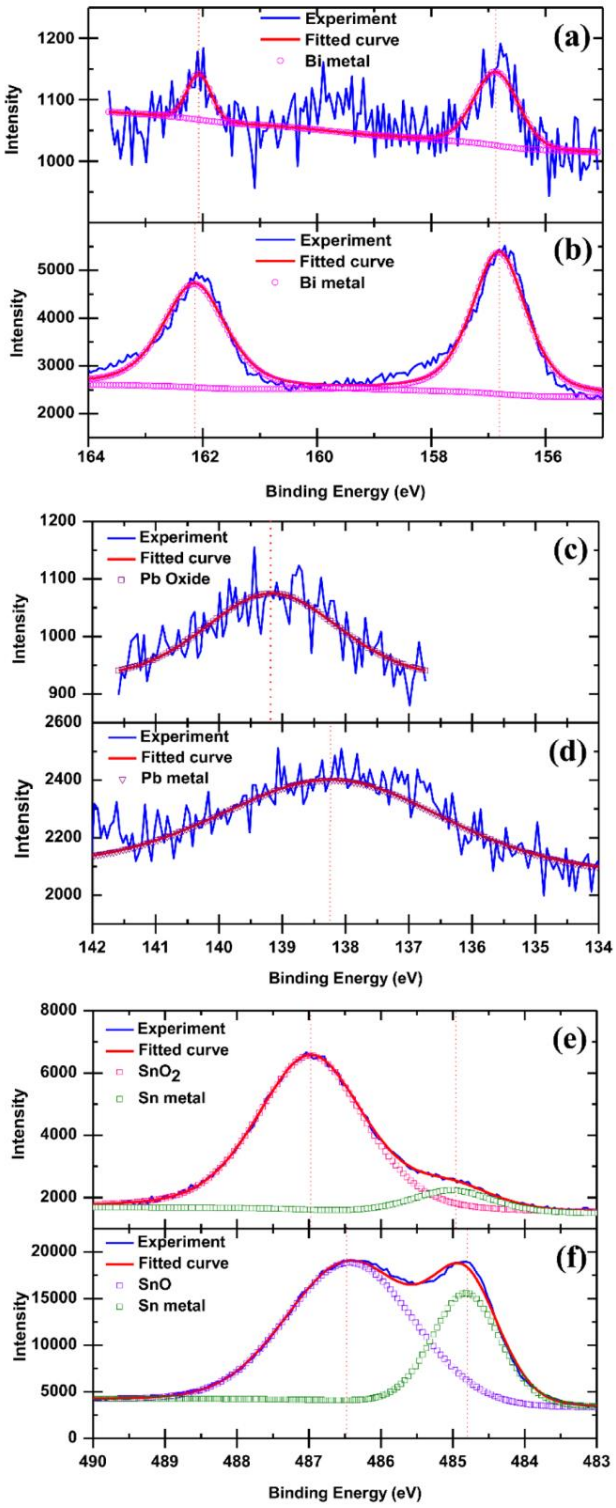

Fig. 9. XPS result of Sn-4%wtBi alloy (a, b) Bi element, (c, d) Pb element and (e, f) Sn element as (a, c, e) non-polished sample and (b, d, f) polished sample.

In hard disk drive manufacturing process before diamond embedding process, lapping plate surface was lathed to smoothen the surface and to get rid oxides on the surface. This is because nanometer-thickness level of oxides on the surface obstruct diamond charging and alter the mechanical properties in the nano-scale. XPS was used to analyze the oxide thickness and species. The results were shown in Fig. 9. Tin oxide and small amount of contaminated lead oxide were founded on the surface of these alloys. Bismuth did not

form bismuth oxide on the surface. Binding energies of Sn $3d_{5/2}$ in SnO and SnO_2 are about 486.5 eV and 487.2 eV respectively [27, 28]. Binding energy of Bi $4f_{7/2}$ in Bi metal is about 157.0 eV [29]. XPS result of Pb is not obvious because of its low content. However, binding energy of Pb $4f_{7/2}$ in Pb oxide may assume that deviation from Pb metal is about 1.5 eV [30]. From the thermodynamic view point, Gibbs free energy for oxide formation of lead has a lower value than those of tin oxide and bismuth oxide. Aside from SnO_2, after polishing, the surface of samples also revealed another species of tin oxide corresponding to SnO. This agrees well with the literature as SnO_2 prefers to form at higher temperature near 573K (300°C) while SnO forms at room temperature [31].

4. Conclusion

The microstructure and mechanical properties of pure Sn and Sn-4%wtBi alloy samples produced by permanent mold gravity casting and forging process were investigated. The addition of 4 wt% Bi into the Sn alloy showed grain refinement effect. Bi precipitates were found along grain boundaries for as-cast samples. At 0.25 strain, the deformation energy may not be enough for driving recrystallization at room temperature however, when the strain reaches 0.5, there were evidences for grain growth and clustering of grains of similar grain boundary misorientation angles. As a result, coarser microstructure was found for the case of 0.5 strain samples. For all cases, as grain sizes decreased, the hardness values increased, following the Hall-Petch relationship. However, in Sn-4%wt.Bi alloy the hardness values were also contributed by solid solution and precipitation strengthening mechanisms. SnO_2 and Pb oxide were found on the surface of these alloys after casting process. Pb content remained however in just the trace level. After polishing, SnO was found on the surface as it could be formed at the room temperature. Bi oxide was not found.

Acknowledgements

The authors would like to acknowledge the financial support from Office of the Higher Education Commission. We thank the Synchrotron Light Research Institute (Public Organization), SUT-NANOTEC-SLRI XPS, Nakhon Ratchasima, Thailand for providing XPS facility and the Department of Physics, Khon Kaen University for XRD facility.

Reference

[1] B. L. Silva, G. Reinhart, H. Nguyen-Thi, N. Mangelinck-Noël, A. Garcia, and J. E. Spinelli, "Microstructural development and mechanical properties of a near-eutectic directionally solidified Sn–Bi solder alloy," *Materials Characterization*, vol. 107, pp. 43-53, 2015.

[2] K. Dhanapal, V. Narayanan, and A. Stephen, "Influence of Sn on the magnetic ordering of Ni–Sn alloy synthesized using chemical reduction method," *Journal of Magnetism and Magnetic Materials*, vol. 406, pp. 103-109, 2016.

[3] Y. Mitsui, K. Oikawa, K. Koyama, and K. Watanabe, "Thermodynamic assessment for the Bi–Mn binary phase diagram in high magnetic fields," *Journal of Alloys and Compounds*, vol. 577, pp. 315-319, 2013.

[4] Z. L. Ma, S. A. Belyakov, and C. M. Gourlay, "Effects of cobalt on the nucleation and grain refinement of Sn-3Ag-0.5Cu solders," *Journal of Alloys and Compounds*, vol. 682, pp. 326-337, 2016.

[5] D. H. Cho, J. H. Nam, B. W. Lee, K. M. Cho, and I. M. Park, "Effect of Mn addition on grain refinement of biodegradable Mg4Zn0.5Ca alloy," *Journal of Alloys and Compounds*, vol. 676, pp. 461-468, 2016.

[6] A. F. da Silveira, W. B. de Castro, B. A. Luciano, and C. S. Kiminami, "Microstructure of under-cooled Sn–Bi and Al–Si alloys," *Materials Science and Engineering: A*, vol. 375–377, pp. 473-478, 2004.

[7] R. Gupta, S. Srivastava, N. K. Kumar, and S. K. Panthi, "High leaded tin bronze processing during multi-directional forging: Effect on microstructure and mechanical properties," *Materials Science and Engineering: A*, vol. 654, pp. 282-291, 2016.

[8] G. M. Castro Güiza and C. A. S. Oliveira, "Microstructural changes produced by hot forging in a C300 Maraging Steel," *Materials Science and Engineering: A*, vol. 655, pp. 142-151, 2016.

[9] *Standard Test Methods for Determining Average Grain Size*, ASTM Standard, 1996.

[10] R. Mahmudi, A. R. Geranmayeh, S. R. Mahmoodi, and A. Khalatbari, "Room-temperature indentation creep of lead-free Sn-Bi solder alloys," *Journal of Materials Science: Materials in Electronics*, vol. 18, pp. 1071-1078, 2007.
[11] T. B. Massalski, H. Okamoto, P. R. Subramanian, and L. Kacprzak, *Binary Alloy Phase Diagrams*, 2nd ed. Materials Park, OH, USA: ASM International, 1990, p. 512.
[12] D. Swenson, "The effects of suppressed beta tin nucleation on the microstructural evolution of lead-free solder joints," *Journal of Materials Science: Materials in Electronics*, vol. 18, no. 1-3, pp. 39-54, 2007.
[13] K. Sweatman, S. D. Mcdonald, M. Whitewick, T. Nishimura, and K. Nogita, "Grain refinement for improved lead–Free solder joint reliability," in *IPC APEX EXPO Conference and Exhibition 2013, APEX EXPO 2013 - San Diego, CA*, pp. 561-589.
[14] R. D. Doherty, G. Gottstein, J. R. Hirsch, W. B. Huttchinson, K. Lucke, E. Nes, and P. J. Wilbrandt, "Panel discussion on recrystallization texture," in *ICO-TOM8*, TMS, Warrendale, PA, 1988. J.S. Kallend and G. Gottstein, Eds., p. 369.
[15] R. D. Doherty, D. A. Hughes, F. J. Humphreys, J. J. Jonas, D. Juul Jensen, M. E. Kassner, W. E. King, T. R. McNelley, H. J. McQueen, and A. D. Rollett, "Current issues in recrystallization: A review," *Materials Science and Engineering: A*, vol. 238, pp. 219-274, 1997.
[16] J. W. Martin, R. D. Doherty, and B. Cantor, *Stability of Microstructure in Metallic Systems*, vol. 2. Cambridge: Cambridge University Press, 1997.
[17] X. Li, H. Sun, P. Zhang, and W. Fang, "The effect of strain on dynamic recrystallization of PM Ti-45Al-10Nb intermetallics during isothermal forging," *Intermetallics*, vol. 55, pp. 90-94, 2014.
[18] J. Zhang, W. Li, and Z. Guo, "Static recrystallization and grain growth during annealing of an extruded Mg-Zn-Zr-Er magnesium alloy," *Journal of Magnesium and Alloys*, vol. 1, pp. 31-38, 2013.
[19] A. H. Cottrell, *Progress in Metal Physics*. 1953.
[20] N. Arora and B. R. Jagirdar, "From (Au5Sn + AuSn) physical mixture to phase pure AuSn and Au5Sn intermetallic nanocrystals with tailored morphology: Digestive ripening assisted approach," *Phys Chem Chem Phys,* vol. 16, pp. 11381-9, Jun. 2014.
[21] J. K. Mason and C. A. Schuh, "The Generalized Mackenzie Distribution: Disorientation angle distributions for arbitrary textures," *Acta Materialia,* vol. 57, pp. 4186-4197, 2009.
[22] V. Y. G. O.V. Mishin, R. Z. Valiev, and G. Gottstein, "Grain boundary distribution and texture in ultrafine-grained copper produced by severe plastic deformation," *Scripta Materialia,* vol. 35, pp. 873-878, 1996.
[23] Y. C. Lin, D.-G. He, M.-S. Chen, X.-M. Chen, C.-Y. Zhao, X. Ma, and Z. L. Long, "EBSD analysis of evolution of dynamic recrystallization grains and δ phase in a nickel-based superalloy during hot compressive deformation," *Materials & Design*, vol. 97, pp. 13-24, 2016.
[24] M. Hatherly, "Recrystallization '90," in *TMS*. Warrendale, PA, 1990, p. 59.
[25] N. Hansen, "Hall–Petch relation and boundary strengthening," *Scripta Materialia,* vol. 51, pp. 801-806, 2004.
[26] S. R. S. Serope Kalpakjian, *Manufacturing, Engineering & Technology*, 2006.
[27] M. Fondell, M. Gorgoi, M. Boman, and A. Lindblad, "An HAXPES study of Sn, SnS, SnO and SnO_2," *Journal of Electron Spectroscopy and Related Phenomena*, vol. 195, pp. 195-199, 2014.
[28] D. A. Zatsepin, A. F. Zatsepin, D. W. Boukhvalov, E. Z. Kurmaev, and N. V. Gavrilov, "Sn-loss effect in a Sn-implanted a-SiO_2 host-matrix after thermal annealing: A combined XPS, PL, and DFT study," *Applied Surface Science,* vol. 367, pp. 320-326, 2016.
[29] B. Oprea, T. Radu, and S. Simon, "XPS investigation of atomic environment changes on surface of B2O3–Bi2O3 glasses," *Journal of Non-Crystalline Solids,* vol. 379, pp. 35-39, 2013.
[30] Z. Su, Q. Wang, J. Li, and G. Zhang, "Self-sacrifice Te template synthesis of new phase PbmSb2nTem+3nnanorods via Pb2+/Sb3+synergistic effect," *RSC Adv.,* vol. 5, pp. 105379-105392, 2015.
[31] Z. Wang, H. A. Al-Jawhari, P. K. Nayak, J. A. Caraveo-Frescas, N. Wei, M. N. Hedhili, and H. N. Alshareef, "Low temperature processed complementary metal oxide semiconductor (CMOS) device by oxidation effect from capping layer," *Sci Rep*, vol. 5, p. 9617, 2015.